1D and 2D NMR spectroscopy of bonding interactions within stable and phase-separating organic electrolyte–cellulose solutions

Matthew T. Clough,[a] Christophe Farès*[a] and Roberto Rinaldi*[b]

Abstract: Organic electrolyte solutions (mixtures containing an ionic liquid and a polar, molecular co-solvent) are highly versatile solvents for cellulose. However, the underlying solvent–solvent and solvent–solute interactions are not yet fully understood. Herein, mixtures of the ionic liquid 1-ethyl-3-methylimidazolium acetate, the co-solvent 1,3-dimethyl-2-imidazolidinone, and cellulose are investigated using 1D and 2D NMR spectroscopy. The use of a triply-^{13}C-labelled ionic liquid enhances the signal-to-noise ratio for ^{13}C NMR spectroscopy, enabling changes in bonding interactions to be accurately pinpointed. Current observations reveal an additional degree of complexity regarding the distinct roles of cation, anion and co-solvent toward maintaining cellulose solubility and phase stability. Unexpectedly, the interactions between the dialkylimidazolium ring C^2–H substituent and cellulose become more pronounced at high temperatures, counteracted by a net weakening of acetate–cellulose interactions. Moreover, for mixtures that exhibit critical solution behaviour, phase separation is accompanied by the apparent recombination of cation–anion pairs.

Introduction

Cellulose is an attractive feedstock for the production of textile fibres[1] or nanocomposite products.[2] However, the toxicity[3] or thermal instability[4] of solvents associated with existing industrial procedures indicates the pressing need for fundamental and applied research towards environmentally-benign technologies for the production of high-performance cellulosic materials. In recent years, organic electrolyte solutions (OESs, incorporating both an ionic liquid, IL, and polar molecular co-solvent) have emerged as promising and versatile solvents for cellulose, offering the simultaneous benefits of rapid dissolution,[5] low viscosity,[6] improved thermal stability[7] and tailorable properties (e.g. reversible phase separation[8]). Favourable thermodynamics and acceptable kinetics are prerequisites for cellulose to dissolve in an OES. If, on the one hand, the free energy of mixing ($\Delta_{mix}G$) remains negative despite dilution of the ions by the co-solvent,[9] cellulose dissolution may nevertheless be *faster* in an OES due to accelerated mass transport of the ions and their more rapid diffusion into the microfibrils.

From a mechanistic perspective, as for pure ILs,[10] it is widely believed that the formation of strong (and directional) hydrogen bonds between the anions and cellulose drives the process of dissolution in an OES.[11] Nevertheless, it is also known that the cation is not merely a spectator and does contribute towards enabling cellulose solubility (via participation in non-directional interactions).[12] Although ion pairs appear to behave as if 'loosened' in [C_4C_1im]Cl–DMSO OESs,[11a-c,13] it has been suggested that DMSO instead improves mass transport of the ions without significant perturbation of the ion–ion interactions.[11d,14] In spite of these interesting preliminary data, there is still uncertainty regarding the precise contributions of cations and anions in promoting and maintaining cellulose solubility. Moreover, previous investigations (e.g. Molecular Dynamics) have commonly focused on one (or only a few) compositions and temperatures. Therefore, changes in the bonding interaction properties of the ions and co-solvent as a function of these variables are not yet established. A clearer understanding of the interplay between the ions and co-solvent could aid in the choice of appropriate IL–co-solvent combinations for future OES–cellulose technologies, both for OES–cellulose mixtures that exist as a stable homogenous phase, and for those that exhibit critical solution behaviour.[8]

Until now, the scientific community has broadly understood that H-bonding interactions between IL anions and the hydroxy substituents of cellulose act as the determining factor for stabilisation of the polymer in an IL or OES solvent. Whilst such bonding interactions are undoubtedly present, in this article, we revisit to what extent ion–ion and ion–solute interactions are perturbed by changes in the solvent composition (dilution of ions), cellulose loading and temperature, with the aim of better understanding the dynamic roles of solvent species. Considering other biomacromolecular systems that are stabilised in solution by hydrogen bonds, DNA (for example) denatures concomitantly with the loosening of hydrogen-bonding interactions between complementary base pairs as the temperature is raised.[15] Conversely, cellulose solubility in IL-based systems is often retained across a broad temperature range, and sufficiently favourable interactions between solvent and solute are maintained.

Therefore, to gain insight into the influence of temperature and solution composition on the specific interactions that underpin cellulose dissolution, as well as another phenomenon recently reported by our research group – reversible phase separation of OES-cellulose solutions[8] – we undertook 1D (^{13}C, ^{1}H) and 2D (^{1}H-^{1}H Nuclear Overhauser Effect) NMR experiments on a series of (binary and) ternary mixtures incorporating 1-ethyl-3-methylimidazolium acetate ([C_2C_1im][OAc]), 1,3-dimethyl-2-imidazolidinone (DMI) and cellulose. This specific combination of IL and co-solvent was chosen in order to be able to study both non-separating and phase-separating mixtures within a series. This paper is divided into two sections. In the first, 1D ^{13}C NMR experiments were carried out for *stable* mixtures (no phase separation in the range 30–90 °C), employing a triply-^{13}C-labelled IL, to examine the influence of solvent composition, cellulose loading and temperature on the interplay of (hydrogen-bonding) interactions. In the second section, variable-temperature 1D and 2D (Nuclear Overhauser Effect) NMR spectroscopy were used to probe the bonding interaction changes associated with the phase separation boundary, for two *phase-separating* mixtures.

[a] Dr. M. T. Clough and Dr. C. Farès
Max-Planck-Institut für Kohlenforschung
Kaiser-Wilhelm-Platz 1, 45470 Mülheim-an-der-Ruhr, Germany
Email: fares@kofo.mpg.de
[b] Dr. R. Rinaldi
Department of Chemical Engineering
Imperial College London, SW7 2AZ, London, UK
Email: rrinaldi@imperial.ac.uk

Supporting information for this article is given via a link at the end of the document.

Overall, this investigation reveals an added degree of complexity regarding the temperature and composition dependency of cation–cellulose and anion–cellulose interactions within IL and OES solvents.

Results and Discussion

NMR spectroscopy of bonding interactions within stable organic electrolyte–cellulose solutions

Initially, in order to pinpoint and differentiate the specific modes of cation and anion interaction with cellulose, three ^{13}C markers were positioned within the IL structure. Therefore, changes in the chemical shift ($\Delta\delta$) of each marker as a result of cellulose dissolution would indicate the *net* change in the number or strength of interactions (solvent–solvent interactions broken, solvent–solute interactions formed), *i.e.*, a net change in electron density in the chemical environment of each ^{13}C marker. A triply-^{13}C-labelled sample of [C_2C_1im][OAc] (denoted IL*) was synthesised (Scheme S1 in the Supporting Information, SI). The ^{13}C NMR chemical shifts of ^{13}C-enriched carboxyl, imidazolium C^2, and imidazolium *N*-methyl substituents are hereafter denoted 'δ_{OAc}', 'δ_{C2}' and 'δ_{Me}', respectively. These substituents were chosen purposefully so as to compare the directional and specific interactions of the acetate anion (δ_{OAc}) versus non-directional and non-specific[10c,10d] interactions of the cation (δ_{C2}, δ_{Me}). Moreover, ^{13}C atoms exhibit sharp and well-resolved signals (compared to ^{1}H and quadrupolar nuclei such as $^{35/37}Cl$), thus enabling accurate monitoring of changes in electronic environments and minimising the length of time samples had to be exposed to temperatures approaching the thermal stability limit.[7]

Three 'blank' solvents (IL*–DMI) were first prepared (mixtures *i-iii*, Table 1, entries *i–iii*, Experimental section). To determine the influence of temperature on the chemical shifts of the blanks (δ_{OAc}, δ_{C2} and δ_{Me}), ^{13}C NMR spectra were obtained at 10 °C increments in the range 30–90 °C. Next, microcrystalline cellulose (MCC) was added to the blank solvents (to χ_{MCC} = 0.02), samples were agitated with gentle heating (≤50 °C) until all cellulose had dissolved by visual inspection, and the variable-temperature NMR experiments were repeated (mixtures *iv-vi*). To mixtures *iv* and *v*, a further aliquot of MCC was added (to χ_{MCC} = 0.06) to afford mixtures *vii* and *viii*, and the variable-temperature NMR experiments were once again repeated. The changes in chemical shifts solely as a result of the inclusion of MCC, $\Delta\delta$, were calculated by subtracting the δ value of the corresponding blank solvent (at the same temperature) (Figs. 1 and 2; $\Delta\delta_{Me}$ graphs are shown in the SI, Fig. S5).

Figure 1 reveals several features. Most importantly, for all of the investigated mixture compositions, the magnitudes of $\Delta\delta_{OAc}$ diminished as a function of increasing temperature, suggesting a clear weakening of acetate–cellulose (hydrogen-bonding) interactions. Counteracting $\Delta\delta_{OAc}$, magnitudes of $\Delta\delta_{C2}$ were observed to increase (or plateau) with increasing temperature, indicating a likely net strengthening (or increase in number) of interactions proximal to the imidazolium C^2 atom. Therefore, the data reveals an interesting temperature-dependent synergy between cation–cellulose and anion–cellulose interactions (Fig. 2). Magnitudes of $\Delta\delta_{Me}$ were typically far smaller than $\Delta\delta_{OAc}$ and $\Delta\delta_{C2}$ at the equivalent temperature and composition (Fig. S5).

For each solvent composition, addition of further MCC (from χ_{MCC} = 0.02 to 0.06) brought about an approximately proportional increase in $\Delta\delta$ (all ^{13}C-enriched substituents), owing to a

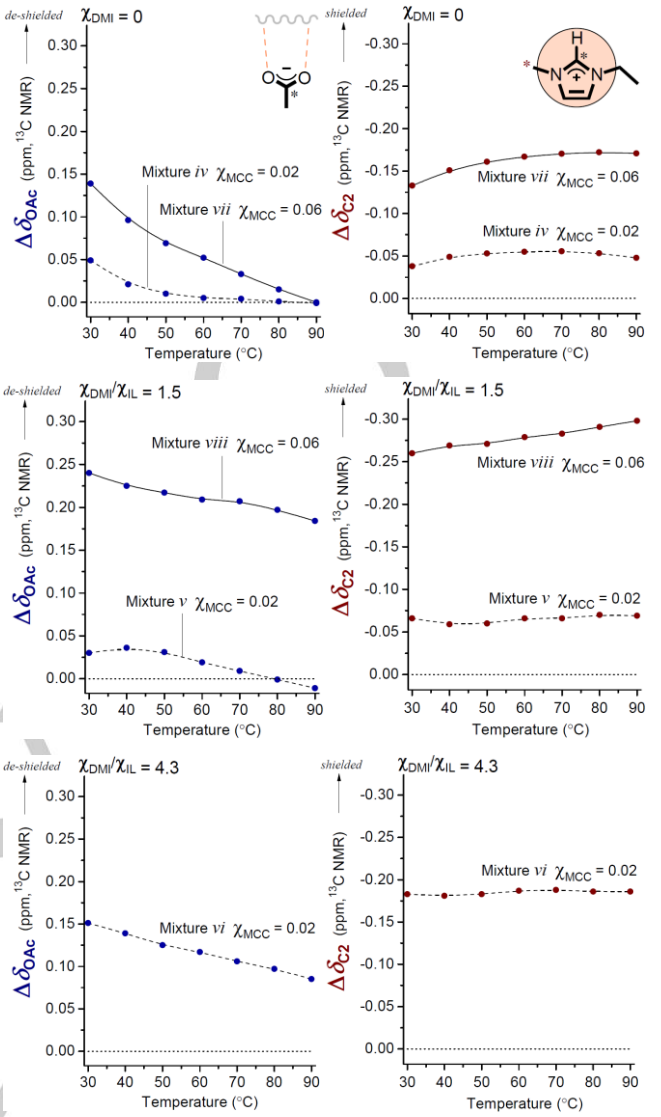

Figure 1. Changes in ^{13}C NMR chemical shifts, $\Delta\delta_{OAc}$ and $\Delta\delta_{C2}$, as a result of addition of microcrystalline cellulose, MCC: (upper) neat IL*; (middle) χ_{DMI}/χ_{IL} = 1.5; (lower) χ_{DMI}/χ_{IL} = 4.3. Precise mixture compositions are listed in Table 1 in the Experimental section. These mixtures exist as a single stable phase in the range 30–90 °C (no phase separation).

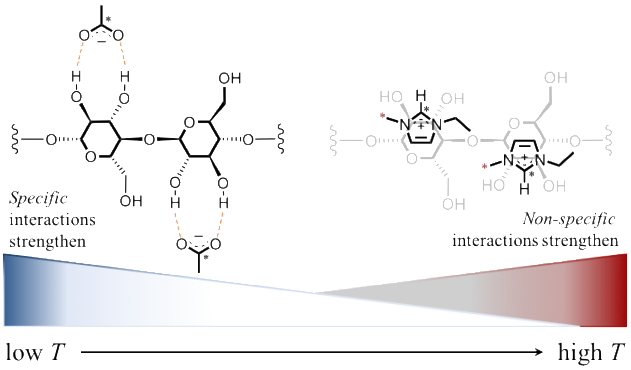

Figure 2. Schematic representation of the proposed cooperative effect between (specific) anion–cellulose and (non-specific[10c]) cation–cellulose interactions as a function of temperature for IL*(–DMI)–MCC mixtures.

proportionally greater fraction of ions interacting closely with cellulose. Similarly, on the transition from IL to OES solvents (ion dilution), the $\Delta\delta$ values typically increased in magnitude, as a greater proportion of ions in the bulk solvent must participate in cellulose interactions, compared to the pure IL. Indeed, magnitudes of $\Delta\delta$ represent weighted average values for ^{13}C atoms that are participating in interaction with cellulose chains against those in the bulk liquid (non-interacting).

In summary, the current results provide evidence regarding the temperature-dependent behaviour of the strengths of the cation–cellulose and anion–cellulose interactions. As depicted in Figure 2, whereby the $[C_2C_1im]^+$ ions play an increasingly important role in cellulose solubility approaching temperatures relevant to traditional large-scale (e.g. electrospinning) applications (≥ 80 °C). Interestingly, at low concentration of IL, the seemingly independent responses of the anion ($\Delta\delta_{OAc}$) and cation ($\Delta\delta_{C2}$) to changes in temperature (e.g., mixture *vi*, χ_{DMI}/χ_{IL} = 4.3, Fig. 1) suggests that the ion pairs behave as though loosened in these non-phase-separating OES–cellulose mixtures.

NMR spectroscopy of bonding interactions within phase-separating organic electrolyte–cellulose solutions

The above-described experiments (Fig. 1) were performed on mixtures existing as a single liquid phase in the range 30–90 °C. However, we recently demonstrated reversible phase separation for mixtures incorporating $[C_2C_1im][OAc]$, DMI and microcrystalline cellulose.[8] Such mixtures fall within a narrow band of composition, characterised by particularly low values of χ_{IL} (shown in Fig. S4 in the SI, and in Table 1 of the Experimental section, below). Above a well-defined 'temperature of phase separation', T_{PS}, the mixtures exist as a single low-viscosity phase, yet upon cooling, they pass through a cloud point and then segregate into distinct IL- and cellulose-enriched lower and DMI-enriched upper layers. Considering these mixtures from a thermodynamic perspective, the interplay of enthalpy and entropy must ultimately control the phase stability. If in any instance χ_{IL} falls below a certain threshold, ΔH can no longer satisfy the criterion $\Delta G < 0$ for spontaneous dissolution of cellulose ($\Delta G = \Delta H - T\Delta S$). However for a mixture with a molar composition close to this boundary, if the temperature is reduced (and $T\Delta S$ falls), then also ΔG may become positive, and cellulose dissolution can no longer be maintained within a single-phase system. In this circumstance, the dissolved cellulose prefers an IL-enriched medium, with the partial exclusion of the DMI co-solvent.

Despite demonstrating this proof-of-concept, the physical and bonding properties underpinning phase separation have not yet been elucidated. Therefore, we decided to explore these systems, undertaking 1D and 2D NMR experiments designed to reveal the changes in ion–ion, ion–co-solvent and ion–cellulose interactions. Phase-separating mixtures were prepared via a previous method (using unlabelled IL),[8] and experimental details are described in the SI.

Initially, a series of 1D ^1H NMR spectra were obtained upon controlled cooling of a phase-separating cellulose solution from 100 to 25 °C (Fig. 3). Upon cooling below the 'phase separation temperature' (T_{PS}) of 61.8 °C, the mixture partitioned into two phases, whereupon the phase boundary then fell within the NMR detection window.

A variety of resonance lines were distinguishable in the imidazolium C^2–H region (10.2–9.6 ppm) including peak and satellite '1'. At high temperatures, a substantial broadening of peak 1 was observed, attributable to the dynamic exchange of the labile C^2–H with labile protons of residual water (confirmed by a negative cross-peak in the NOESY spectrum for related mixture *x*, Table 1). Furthermore, as the mixture cooled approaching TPS, a new shoulder (2) emerged (visible in the spectrum collected at ca. 66 °C), and gradually resolved into a sharp, separate peak '2' at ca. 9.7 ppm (25 °C). This observation indicates a further dynamic exchange effect, whereby at higher temperatures the cations transition between two states (e.g., interacting with or distant from cellulose) at a rate on the order of their chemical shift difference (ca. 200 Hz). A reduction in temperature therefore brings about gradual resolution into distinct peaks. The exchange between the two states represented by peaks 1 and 2 is also observed as negative "exchange" cross-peaks in the NOESY at 50 °C in Fig 4 (described below). The segregation of the cation into one of two distinct chemical environments could be the basis for the macroscopic phase separation (cf. 1D axes of spectra in Fig. 4). Minor peaks '3' and '4' were observed at all temperatures and in a control experiment of blank commercial $[C_2C_1im][OAc]$; 3 and 4 therefore likely correspond to low concentrations of an impurity, possibly C^4 and C^5 ring protons of 1-ethyl-3-methylimidazolium-2-carboxylate.[16]

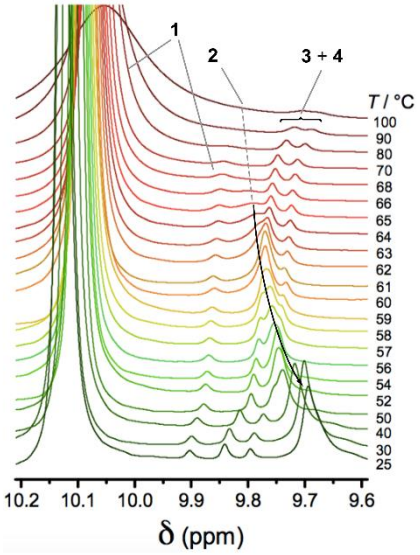

Figure 3. Temperature-dependence of the downfield ^1H NMR spectrum (500 MHz) for phase-separating $[C_2C_1im][OAc]$–DMI–MCC mixture *ix* (Table 1, initial composition χ_{IL} = 0.094, χ_{DMI} = 0.893, χ_{MCC} = 0.013; T_{PS} = 61.8 °C). The spectra were obtained in the direction of cooling from 100 to 25 °C.

In order to more closely pinpoint changes to ion–ion and ion–co-solvent interactions occurring upon phase separation, 2D 'Nuclear Overhauser Effect' (NOE) spectroscopy experiments (interaction of ^1H nuclei through space[17]) were performed on a different phase-separating $[C_2C_1im][OAc]$–DMI–MCC mixture (*x* in Table 1, T_{PS} = 50.2 °C), chosen on the basis that the quantities of upper and lower phases after phase separation were approximately equal,[8] allowing the layers to be decanted easily

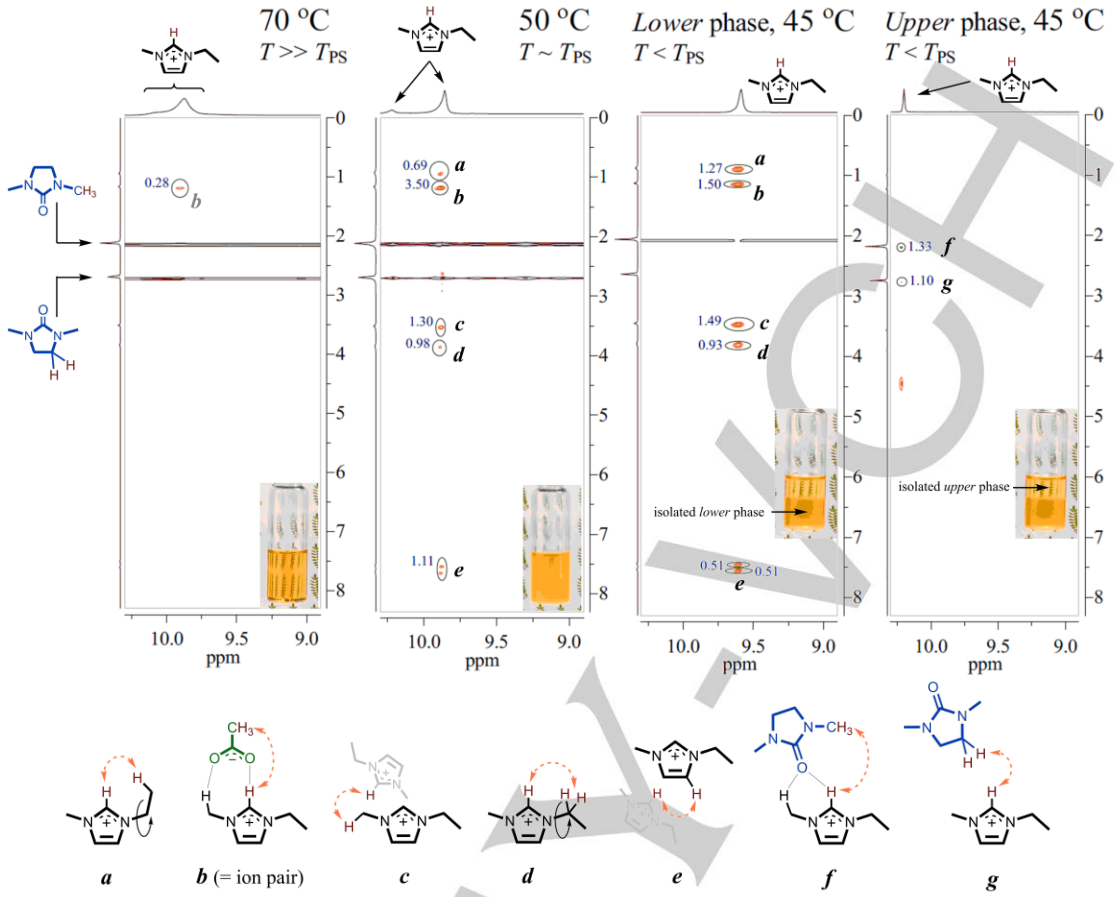

Figure 4. Expanded regions of two-dimensional ^{1}H-^{1}H NOE NMR spectra (400 MHz, DMSO-d6 inserts) for phase-separating [C_2C_1im][OAc]–DMI–MCC mixture *x* (Table 1, initial composition χ_{IL} = 0.167, χ_{DMI} = 0.782, χ_{MCC} = 0.051; T_{PS} = 50.2 °C), from left to right: single phase at 70 °C; onset of phase separation at 50 °C; isolated lower phase at 45 °C, and; isolated upper phase at 45 °C. Proposed interaction motifs '***a***'–'***g***' are displayed beneath the spectra, and the inset pictures indicate the visual appearance of the sample at the specified temperature.[8] The integrals of cross-peaks were calibrated against the integral of the C^{4}H···HC^5 imidazolium intra-ring signal, with fixed inter-nuclear distance (∫ = 1.00).

from one another without cross-contamination. Spectra were obtained at 70 °C (>>T_{PS}), at 50 °C (≈T_{PS}), and for the decanted layers at 45 °C (<T_{PS}) (Fig. 4, full spectra in Fig. S6 of SI). Distinct cross-peaks were readily identified in the imidazolium C^2–H region of the NOE spectra (motifs ***a***–***g***, Fig. 4). Semi-quantification was achieved by calibrating against the imidazolium C^{4}H···HC^5 intra-ring signal of the same NOE spectrum, with a fixed inter-nuclear distance (set as ∫ = 1.00).

A comparison of the 70 °C and 50 °C NOE spectra indicates a significant difference in the ion–ion interaction patterns. At the cloud point (50 °C), distinct cation–cation (***a***, ***c***–***e***) and cation–anion (***b***) cross-peaks were visible, involving the hydrogen-bond-acidic imidazolium C^2 proton. Peaks ***a***, ***c*** and ***d*** may include an intramolecular element between the imidazolium C^2–H and *N*-alkyl protons. However, peaks ***b*** and ***e*** clearly indicate intermolecular cation–anion and cation–cation interactions, respectively, suggesting that the IL ions are in close or prolonged contact with one another at ~T_{PS}. Signal ***b*** (∫ = 3.50) was significantly more intense than signal ***e*** (∫ = 1.11), indicating a clear preference for front–front cation–anion pairs at 50 °C. By contrast, signal ***b*** for the 70 °C measurement is indistinct (∫ = 0.28). NOE peaks depend on close (typically ≤5 Å) and prolonged contact of protons through space. Therefore, it is possible that lower viscosity contributes to the lack of a distinct cation–anion cross-signal at 70 °C. Nevertheless considering the collective observations from Fig. 1 (cations and anions behave as if separated), Fig. 3 (cation rapidly exchanges between two chemical environments >T_{PS}) and Fig. 4 (strong or prolonged cation–anion pairing visible at ~T_{PS}), it is apparent that, for the [C_2C_1im][OAc]–DMI–MCC mixtures, division into two phases is accompanied by recombination of ion pairs.[8]

Examining the spectra of the separated phases at 45 °C, in the IL-rich lower phase, ordered cross-peaks were clearly visible between all cation ring protons and all other IL peaks (Fig. 4, Fig. S6c). The integrals of signals ***a***–***d*** are similar, indicating that the concentration of IL in the lower phase is sufficiently high such that cations are in close contact with neighbouring cations. By contrast, in the DMI-rich upper phase (χ_{DMI}/χ_{IL} = 12.5[8]), ion–ion bonding interactions were absent or very weak, replaced by faint signals for contact between ions and DMI (***f***, ***g***, see also Fig. S6d). Cations and anions, therefore, appear almost wholly separated in the IL-poor upper phase (lack of peak ***b***).

From the 2D NMR data, we propose that cations and anions in non-phase-separating [C_2C_1im][OAc]–DMI–cellulose mixtures behave in an effectively independent or 'loosened' manner, as described in prior literature.[11,14] Cooling of the phase-separating mixture *x* (Fig. 4) brought about the appearance or enlargement of cation–cation and cation–anion cross-peaks ***a***–***e***. Whilst simple reduction in temperature could explain this observation (increase in viscosity, reduced ion mobility), the clear preference for front–front cation–anion pairs (peak ***b***) at 50 °C suggests that a genuine recombinational effect is taking place.

Conclusions

In conclusion, by using 1D and 2D NMR spectroscopy, we have demonstrated that the cation–ion and anion–cellulose interaction strengths for ternary mixtures of [C_2C_1im][OAc], DMI, and microcrystalline cellulose are strongly influenced by the temperature, solvent composition and cellulose loading. The contributions of $[C_2C_1im]^+$ and $[OAc]^-$ to biopolymer solvation depend significantly on the temperature, as has also been observed for dissolution of other biomacromolecules (e.g. DNA, enzymes). Strikingly, at the molecular and bonding level, the explanation for the lack of cellulose precipitation at high temperatures (100–120 °C) appears to be the counterbalance of cation and anion bonding interactions. In fact, for both IL and OES solvents in our study, the net bonding interactions between cations and cellulose (measured according to the electron density change at the ring C^2 position) were broadly observed to increase in strength (or number) in line with temperature, counteracted by a net weakening of the anion–cellulose interactions (not necessarily replicated by all OES–cellulose systems). These results serve to reinforce the key role of the IL cations in maintaining cellulose dissolution, also highlighting the influence of composition and temperature on the interaction capabilities of the different solvent species.

Experimental

Table 1 Compositions of the investigated mixtures *i*-*x*, distinguishing between mixtures that do and do not exhibit thermally-triggered phase separation in the range 30–90 °C. MCC mole fractions were calculated according to the moles of glucopyranose residues, RFM ($C_6H_{10}O_5$) = 162.14 g mol^{-1}.

Mixture	Mixture composition			T_{PS} (°C)
	χ_{IL}	χ_{DMI}	χ_{MCC}	
i	1	0	0	*No* phase separation in region of 30-90 °C.
ii	0.39	0.61		
iii	0.19	0.81		
iv	0.98	0	0.02	
v	0.39	0.59		
vi	0.19	0.79		
vii	0.94	0	0.06	
viii	0.37	0.57		
ix	0.094	0.893	0.013	61.8
x	0.167	0.782	0.051	50.2

NMR spectroscopy

All NMR spectra were recorded either on a Bruker Avance III 500 spectrometer equipped with a 5mm BBFO+ probehead and running Topspin 3.2, or on a Bruker Avance 400 spectrometer equipped with a 5mm BBFO+ probehead and running Topspin 2.1. Sample temperatures were calibrated beforehand with 80% ethylene glycol in DMSO-d_6 according to the established protocol.[4] 1D ^{1}H spectra were measured with a simple pulse-acquire experiment ("zg30"). Non-quantitative 1D $^{13}C\{^1H\}$ NMR (125.70 MHz) spectra were recorded with a standard ^{1}H-decoupled pulse-acquire (zgdc30) experiment using 3.3 µs 30°-pulses on the ^{13}C channel and a WALTZ16-decoupling pulse trains on the ^{1}H. A 0.84 s acquisition time (65536 points), 512 transients and a short recycling delay were used. Carbon chemical shift changes are reported in ppm ($\Delta\delta$) after correcting the middle line of the ^{13}C multiplet of DMSO-d_6 (present in a 1-mm insert) at 39.51 ppm in all spectra. 2D-NOESY spectra were recorded with the standard Bruker pulse sequence 'noesygpph' with coherence-selecting gradients, using a 10 µs 90°-pulse on the ^{1}H channel and mixing times varying between 0.7–1.3 s as optimised from T_1-measurements. Matrix sizes of 2048×512 covering 11×11 ppm were acquired with 4 transients per increment and 3.5 s between transients for a total experiment time of 3 h. Processing and integral measurements were conducted in MNova 11.0.

1D ^{13}C NMR spectroscopy to determine $\Delta\delta$ values

A sample of 2-^{13}C-1-ethyl-3-methylimidazolium 1-^{13}C-acetate (IL*, 278 mg, 1.6 mmol) was diluted with commercial 1-ethyl-3-methylimidazolium acetate (*Iolitec*, >95%) (895 mg, 5.3 mmol). The water content of the resultant (dilute) IL* was determined to be 0.96±0.01 wt% by Karl Fischer titration. Separately, a sample of 1,3-dimethyl-2-imidazolidinone (DMI, 5 mL) was distilled using Kügelrohr apparatus, and the water content was determined to be 0.51±0.01 wt% by Karl Fischer titration. 'Blank' solvent mixtures *i*–*iii* (Table 1) were prepared by carefully weighing predetermined quantities of IL* and DMI into 1 mL glass vials (adjusting for residual water). Mixtures were subsequently transferred into NMR tubes equipped with DMSO-d6 inserts. Initially, 'blank' NMR spectra (^{1}H, 500 MHz; $^{13}C\{^1H\}$, 125 MHz) were obtained for mixtures *i*–*iii* at temperatures in the range 30–90 °C (with 10-minute intervals between measurements to allow temperature equilibration). Chemical shifts δ_{C2}, δ_{OAc} and δ_{Me} in the ^{13}C NMR spectra were determined. Subsequently, to each blank mixture, microcrystalline cellulose (MCC, Avicel, DP = ~175) was added up to χ_{MCC} = 0.02, affording mixtures *iv*–*vi* (Table 1). ^{1}H and ^{13}C NMR spectra were obtained for mixtures *iv*–*vi* (as for *i*–*iii*), and changes in chemical shifts arising from the addition of MCC ($\Delta\delta_{C2}$, $\Delta\delta_{OAc}$ and $\Delta\delta_{Me}$) were evaluated. Ternary mixtures *iv* and *v* were then treated with additional cellulose up to χ_{MCC} = 0.06, affording mixtures *vii* and *viii*, respectively (Table 1). NMR spectra were obtained, and the $\Delta\delta_{C2}/\Delta\delta_{OAc}/\Delta\delta_{Me}$ values were calculated for *vii* and *viii*, in analogy to mixtures *iv*–*vi* (described above).

2D NOESY to investigate phase separation

A phase-separating ternary [C_2C_1im][OAc]–DMI–MCC mixture, *x* (initial composition: χ_{IL} = 0.167, χ_{DMI} = 0.782, χ_{MCC} = 0.051, T_{PS} = 50.2 °C) was prepared on a 5.000 g scale, according to a prior method.[5] The mixture was warmed to 70 °C, with vigorous stirring, and was maintained at this temperature until fully homogenous according to visual inspection. A small aliquot (~0.5 g) of the single-phase mixture was extracted with a pre-heated syringe/needle and was transferred to a pre-heated NMR tube with a DMSO-d_6 insert, and the tube was kept in a water bath heated to 70 °C. The sample was transferred to an NMR spectrometer (400 MHz) set at 70 °C, and the NOESY experiment was started.

Measurements were performed at 70 °C (>>T_{PS}) and 50 °C (~T_{PS}) (Fig. 4 and Fig. S6a, b). The remaining fraction of the mixture (~4.5 g) was allowed to settle into two phases at room temperature overnight, and the phases were carefully separated by decanting of the top layer from the bottom (viscous) layer. Small aliquots of the separate phases (~0.5 g) were transferred to NMR tubes fitted with DMSO-d_6 inserts, and NOE spectra were obtained at 45 °C (<T_{PS}) (Fig. 4 and Fig. S6c, d). Semi-quantification of ^{1}H-^{1}H NOESY cross-peaks was performed by calibrating against the imidazolium $C^4H\cdot\cdot HC^5$ intra-ring signal (from IL) with fixed inter-nuclear distance (set at $\int$ = 1.00).

Acknowledgements

This project was undertaken as part of the Cluster of Excellence "Tailor-Made Fuels from Biomass" (DFG).

Keywords: Organic Electrolytes • Ionic Liquids • Cellulose • NMR • Hydrogen bonding

[1] M. Hummel, A. Michud, M. Tanttu, S. Asaadi, Y. Ma, L. J. Hauru, A. Parviainen, A. T. King, I. Kilpeläinen, H. Sixta, in *Ionic Liquids for the Production of Man-Made Cellulosic Fibers: Opportunities and Challenges*, Springer Berlin Heidelberg, **2015**, pp. 1-36.

[2] Y. Habibi, *Chem. Soc. Rev.* **2014**, *43*, 1519-1542.

[3] T. Liebert, *Cellulose Solvents: For Analysis, Shaping and Chemical Modification, Vol. 1033*, American Chemical Society, **2010**.

[4] T. Rosenau, A. Potthast, H. Sixta, P. Kosma, *Prog. Polym. Sci.* **2001**, *26*, 1763-1837.

[5] R. Rinaldi, *Chem. Commun.* **2011**, *47*, 511-513.

[6] a) Y. Lv, J. Wu, J. Zhang, Y. Niu, C.-Y. Liu, J. He, J. Zhang, *Polymer* **2012**, *53*, 2524-2531; b) M. Kostag, T. Liebert, T. Heinze, *Macromol. Rapid Commun.* **2014**, *35*, 1419-1422; c) A. J. Holding, V. Mäkelä, L. Tolonen, H. Sixta, I. Kilpeläinen, A. W. T. King, *ChemSusChem* **2016**, *9*, 880-892.

[7] a) M. T. Clough, J. A. Griffith, O. Kuzmina, T. Welton, *Green Chem.* **2016**, *18*, 3758-3766; b) M. T. Clough, K. Geyer, P. A. Hunt, S. Son, U. Vagt, T. Welton, *Green Chem.* **2015**, *17*, 231-243; c) N. Meine, F. Benedito, R. Rinaldi, *Green. Chem*. **2010**, *12*, 1711-1714.

[8] H. F. N. de Oliveira, M. T. Clough, R. Rinaldi, *ChemSusChem* **2016**, *9*, 3324-3329.

[9] a) H. F. N. de Oliveira, R. Rinaldi, *ChemSusChem* **2015**, *8*, 1577-1584; b) J. M. Andanson, A. A. H. Padua, M. F. Costa Gomes, *Chem. Commun.* **2015**, *51*, 4485-4487.

[10] a) R. C. Remsing, R. P. Swatloski, R. D. Rogers, G. Moyna, *Chem. Commun.* **2006**, 1271-1273; b) H. Liu, G. Cheng, M. Kent, V. Stavila, B. A. Simmons, K. L. Sale, S. Singh, *J. Phys. Chem. B* **2012**, *116*, 8131-8138; c) H. Liu, K. L. Sale, B. M. Holmes, B. A. Simmons, S. Singh, *J. Phys. Chem. B* **2010**, *114*, 4293-4301; d) H. M. Cho, A. S. Gross, J.-W. Chu, *J. Am. Chem. Soc.* **2011**, *133*, 14033-14041.

[11] a) A. Xu, Y. Zhang, Y. Zhao, J. Wang, *Carbohydr. Polym.* **2013**, *92*, 540-544; b) Y. Zhao, X. Liu, J. Wang, S. Zhang, *J. Phys. Chem. B* **2013**, *117*, 9042-9049; c) F. Huo, Z. Liu, W. Wang, *J. Phys. Chem. B* **2013**, *117*, 11780-11792; d) S. Velioglu, X. Yao, J. Devémy, M. G. Ahunbay, S. B. Tantekin-Ersolmaz, A. Dequidt, M. F. Costa Gomes, A. A. Pádua, *J. Phys. Chem. B* **2014**, *118*, 14860-14869; e) Y.-B. Huang, P.-P. Xin, J.-X. Li, Y.-Y. Shao, C.-B. Huang, H. Pan, *ACS Sustain. Chem. Eng.* **2016**, *4*, 2286-2294.

[12] a) B. D. Rabideau, A. Agarwal, A. E. Ismail, *J. Phys. Chem. B* **2013**, *117*, 3469-3479; b) B. Mostofian, J. C. Smith, X. Cheng, *Cellulose* **2014**, *21*, 983-997; c) B. D. Rabideau, A. Agarwal, A. E. Ismail, *J. Phys. Chem. B* **2014**, *118*, 1621-1629.

[13] A. J. Holding, M. Heikkilä, I. Kilpeläinen, A. W. T. King, *ChemSusChem* **2014**, *7*, 1422-1434.

[14] J.-M. Andanson, E. Bordes, J. Devémy, F. Leroux, A. A. Pádua, M. F. C. Gomes, *Green Chem.* **2014**, *16*, 2528-2538.

[15] a) D. Poland, H. A. Scheraga, *J. Chem. Phys.* **1966**, *45*, 1456-1463; b) D. Poland, H. A. Scheraga, *J. Chem. Phys.* **1966**, *45*, 1464-1469; c) W. Sung, J.-H. Jeon, *Physical Review E* **2004**, *69*, 031902.

[16] M. Smiglak, J. D. Holbrey, S. T. Griffin, W. M. Reichert, R. P. Swatloski, A. R. Katritzky, H. Yang, D. Zhang, K. Kirichenko, R. D. Rogers, *Green Chem.* **2007**, *9*, 90-98.

[17] a) J. Jeener, B. Meier, P. Bachmann, R. Ernst, *J. Chem. Phys.* **1979**, *71*, 4546-4553; b) R. Wagner, S. Berger, *J. Magn. Reson., Ser A* **1996**, *123*, 119-121.

[18] E. Gale, R. H. Wirawan, R. L. Silveira, C. S. Pereira, M. A. Johns, M. S. Skaf, J. L. Scott, *ACS Sustain. Chem. Eng.* **2016**, *4*, 6200-6207.

Entry for the Table of Contents

COMMUNICATION

To me, to you: for organic electrolytes derived from the ionic liquid 1-ethyl-3-methylimidazolium acetate and the co-solvent 1,3-dimethyl-2-imidazolidinone, the contributions of cation and anion towards promoting and maintaining cellulose dissolution are influenced significantly by both temperature and mixture composition.

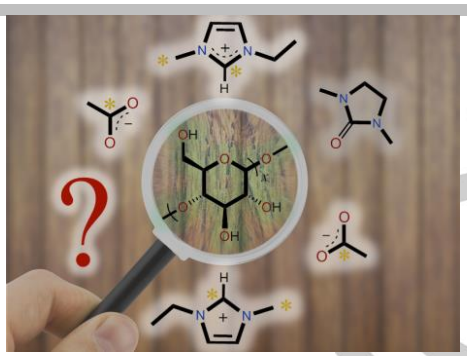

Matthew T. Clough, Christophe Farès and Roberto Rinaldi**

Page No. – Page No.

1D and 2D NMR spectroscopy of bonding interactions within stable and phase-separating organic electrolyte–cellulose solutions